Seismic responses of reinforced concrete frames with buckling restrained braces in zigzag configuration

Zhe Qu [a],[*], Shoichi Kishiki [b], Yusuke Maida [c], Hiroyasu Sakata [b], Akira Wada [b]

[a] Key Laboratory of Earthquake Engineering and Engineering Vibration, Institute of Engineering Mechanics, CEA, Sanhe, Hebei 065201, China
[b] Structural Engineering Research Center, Tokyo Institute of Technology, Nagatsuta, Midori, Yokohama 226-8503, Japan
[c] Graduate School of Engineering, Department of Architecture, Chiba University, 1-33 Yayoi, Inage, Chiba 263-8522, Japan

ABSTRACT

A new buckling restrained braced frame system was proposed in a previous study for reinforced concrete frames, which was featured by the zigzag configuration of buckling restrained braces to ease the steel-to-concrete connection. Experimental tests were conducted to establish realistic numerical models of the brace connections in the proposed system. With these numerical models, a nonlinear dynamic analysis of a prototype building was conducted to investigate the seismic behavior of the new braced frame system. The results indicate that the buckling restrained braces in the new system are efficient in reducing the responses of the building, even if the nonlinearity of the brace connection is considered. Furthermore, the strength demands for the brace connections are significantly influenced by higher modes of the system after the braces yield.

© 2015 Elsevier Ltd. All rights reserved.

1. Introduction

The seismic performance and design of gusset connections are critical for steel braced frame structures. In addition to the brace action that is well addressed in design codes such as AISC 360 [1], corner gusset plates are frequently subjected to 'frame actions,' which can be quite complicated [2,3] and may lead to premature fracture of welds or buckling of gusset plates, thus impairing the seismic performance of the system [4]. It is impractical to include such complicated behavior of gusset connections in structural modeling for routine design purposes. Instead, the braces are usually assumed to be pin-connected to the frame by using truss elements in the structural analyses, such as those conducted by [5,6].

The frame action in gusset connections remains a problem when implementing steel braces in reinforced concrete (RC) frames. In addition to its detrimental effects on the gusset plates, it may also result in considerable over-strength in RC frames [7] and sometimes unfavorable shear failure of adjoining concrete columns [8] by reducing their effective lengths. To make it worse, steel braces in conventional configurations impose large concentrated tensile force on gusset connections. It is not easy to transfer

this force to concrete members because concrete is weak in tension. While fundamental tests were conducted to investigate the performance of steel gusset-to-concrete connections [9,10], new solutions other than conventional corner gusset connections have been proposed, such as that of fastening the gusset plates to the side surfaces of RC beams by post-tensioned steel rods [11–14], and that of anchoring the gusset plates by shear-key plates that are exempt from significant tensile forces [15,16]. Another example is the 'unconstrained gusset connection' on the top surface of RC beams [17], which is an extension of a similar idea for steel frames [18]. Similar connection details was also applied to the BRB-to-pile cap connections in the tests specimens of strengthening non-ductile RC frames with BRBs [19].

Taking advantage of the capacity of buckling restrained braces (BRBs) to develop full plastic strength in both tension and compression [20], a zigzag buckling restrained braced frame system was proposed for RC structures in previous studies (referred to as 'continuously bucking restrained braced frame' in [21,22]). As illustrated in Fig. 1(a), BRBs in the proposed system are arranged in a zigzag layout and those in neighboring stories share the same gusset plate so that they run continuously along the height of the structure. Instead of fitting into the corners of beams and columns, the shared gusset plates are attached to the sides of beam-column joints so that the 'frame action' in conventional corner gusset

* Corresponding author. Tel.: +86 316 3395229; fax: +86 316 3395246.
E-mail address: m.quzhe@gmail.com (Z. Qu).

connections are avoided, making it much easier to determine the capacity demands for connections. This is made possible by eliminating beams in the braced span, which are fundamentally zero-force members if the braced span is considered as a planar cantilevered truss, as demonstrated by a simple example in Fig. 2. In the truss analogy, the removal of vertical zero-force web members has no effect on forces of other members and makes the truss into a 'Warren truss,' which has long been received as an efficient structural system for bridges. It can be equally efficient as a lateral system for building structures when erected vertically, as in the proposed system.

Although beam removal in the braced span would reduce the lateral stiffness and strength of the RC moment frame, this reduction is considered insignificant because the number of braced spans in the entire building is relatively small and most lateral resistance comes from braces rather than moment frames. When necessary, it can be easily compensated by using larger BRBs.

While other connection details may also be available, it is proposed to anchor gusset plates by post-tensioning bolts embedded in beam-column joints along with RC corbels in pair that jut out from columns on both the top and the bottom ends of gusset plates (Fig. 1(b)). The horizontal (i.e., the embedded bolts) and the vertical (i.e., RC corbels) resistances of the connection are essentially independent of each other, so both the bolts and the corbels are under relatively simple load conditions. Therefore, their behavior becomes easier to predict and control.

It would also be beneficial if the two BRBs sharing the same gusset plate yield at the same time but in opposite directions (i.e., one in tension and one in compression) because the horizontal components of their forces can counter-act each other and thus impose very small demand for the horizontal resistance of the connection. In other words, there is a possibility that the connection in the proposed system does not need to be designed against significant tensile force.

In previous studies, cyclic loading tests were conducted on sub-assemblies of zigzag BRBF systems to validate brace connections and to evaluate the performance of adjoining RC components and BRBs [21,22]. In the present study, focus is on the connections as parts of the entire system. Monotonic loading tests are conducted to better understand the load–displacement behavior and the ultimate capacity of connection components, based on which a simple numerical model that reasonably captures the nonlinear behavior of connections is established. The numerical model is integrated into the nonlinear finite element model of a prototype zigzag BRBF building for nonlinear dynamic analysis to clarify the influence of BRB connections on seismic responses of buildings.

2. Experimental tests of proposed connections

As confirmed in a previous study [22], the horizontal and vertical forces on a gusset plate transmitted by BRBs are resisted by bolts and corbels almost independently in the proposed connection, as depicted in Fig. 1(b). This makes it possible to evaluate the connection behavior through separate shear tests of RC corbels and tension tests of post-tensioned bolts. Four tested specimens of zigzag BRBF subassemblies in a previous experimental program, which is documented in details by [21], were re-utilized for this purpose. The specimens were T-shaped and each consisted of a half-span RC beam framing into an RC column, extending half story height above and below the joint, with a gusset plate anchored by embedded bolts and a pair of RC corbels. The beams were unnecessary for the present tests and were cut off before the tests. The cylinder concrete compressive strength of the specimens was 58 MPa, the split tensile strength was 3.5 MPa, and the elastic modulus was 33,000 MPa.

2.1. Reinforced concrete corbel

The RC corbel under investigation is depicted in Fig. 3, which features a very small shear span-to-depth ratio (generally below 0.5). Stirrups are uniformly distributed along the depth of the
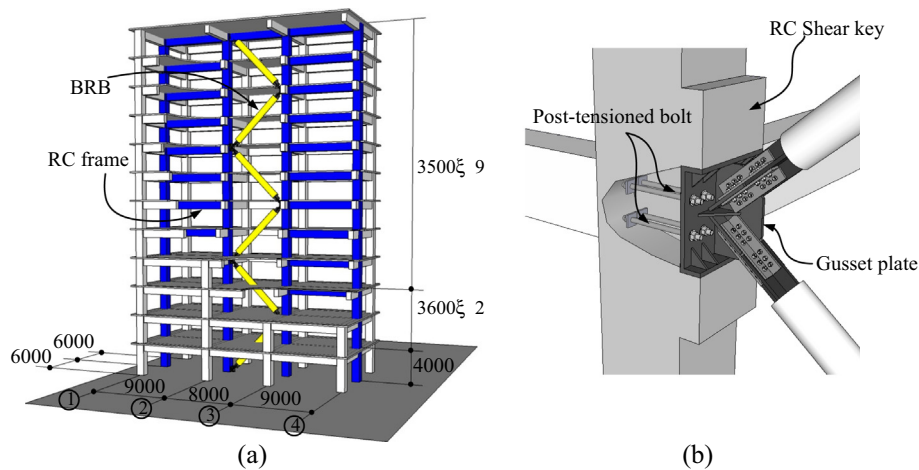

Fig. 1. Zigzag buckling restrained braced RC frame: (a) BRB configuration and (b) details of the BRB connection.
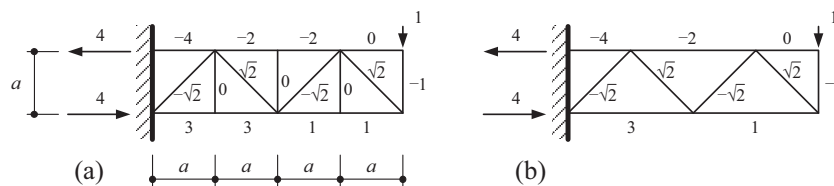

Fig. 2. Truss analogy for a concentrically braced frame: (a) with vertical web members and (b) without vertical web members (Warren truss).
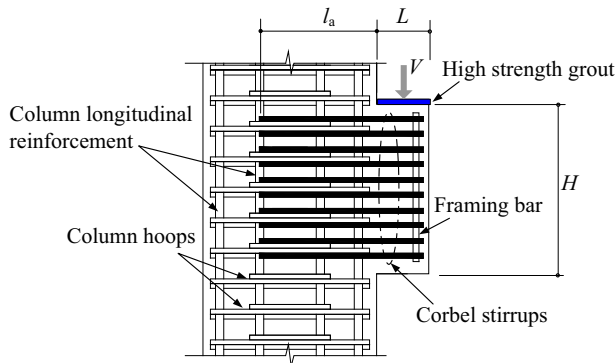
Fig. 3. RC corbel for shear key.

corbel and are anchored inside the column. Four RC corbels on two of the above-mentioned four specimens were tested because they remained essentially un-damaged in the previous tests. All four corbels had identical dimensions as shown in Table 1. The shear span-to-depth ratio, L/H, was 0.175. The yield strength of the ϕ10 stirrups was 346 MPa per material tests. Two corbels were reinforced by a total of 20 legs of stirrups (referred to as C1a and C1b, hereinafter), and two were reinforced by half the amount of

Table 1
Corbel dimensions.

Length, L	70 mm
Depth, H	400 mm
Width, B	400 mm
Anchorage, l_a	270 mm

stirrups (referred to as C2a and C2b, hereinafter). The resultant transverse reinforcement ratio, that is, the ratio of the cross sectional area of all stirrups and that of the corbel ($B \times H$), is 0.98% for C1a and C1b and 0.49% for C2a and C2b.

The self-balanced loading system shown in Fig. 4 was used to subject a single corbel protruding from the column to pure shear. The loading jig was connected to four high-strength steel rods, the other ends of which were connected to a wide-flange steel reaction beam. A hydraulic jack was installed in between the reaction beam resting on a roller cushion and the end of the RC column via a rigid steel connector. During loading, the jack pushed the reaction beam away from the specimen and thus pulled the loading jig to impose shear force on the RC corbel. Monotonic loading was applied until RC corbels were crushed. Two LVDTs were mounted on both sides of the column to monitor the displacement of the loading jig relative to the underneath column.

With increased shear force in corbels, minor cracks initiated from the toes of loading jigs and developed diagonally into corbels before they were suddenly crushed. Fig. 5 depicts the cracks and ultimate failure surface of the specimens. No obvious difference was observed in the failure modes of the two groups of corbels, although their strengths were quite different.

A simple hysteretic model in Fig. 6(a) is assumed for the RC corbels in shear, in which the skeleton curve (described by Eq. (1)) is analogous to the widely used parabolic strain–stress relationship for concrete in compression. In light of the brittle failure observed in the tests, it is assumed that corbels fail as soon as shear force reaches the shear strength, V_u. Before failure, corbels may unload by initial stiffness, K_{c0}, before reaching zero force (see Fig. 6(a)). During reloading, the resistance would not recover until residual deformation in previous loading cycles is exceeded.

$$V = V_u \left[\frac{2\delta}{\delta_0} - \left(\frac{\delta}{\delta_0} \right)^2 \right], V \leqslant V_u \quad (1)$$
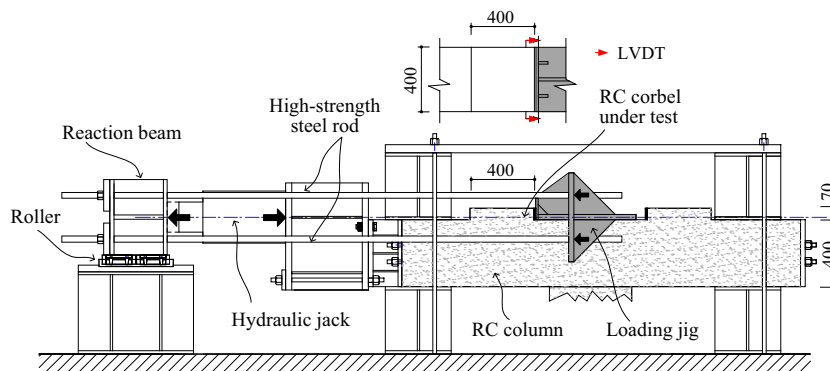

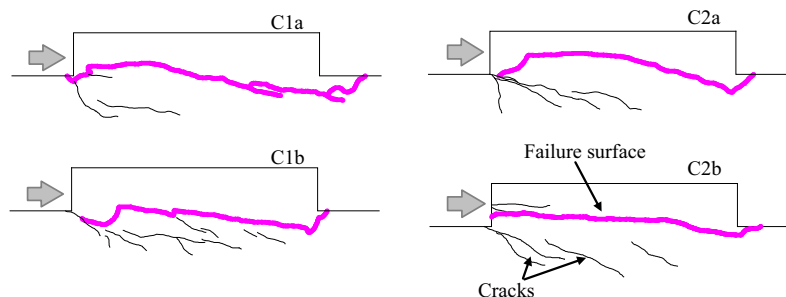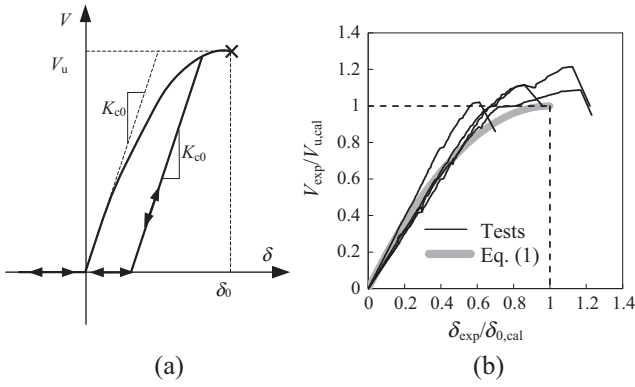**Fig. 4.** Loading setup of corbel shear test.

Fig. 5. Cracks and failure surfaces of RC corbels.

Fig. 6. Corbel behavior: (a) idealized hysteretic model and (b) skeleton curves from tests.

where V and δ are the shear force and the deformation of the corbel, respectively; V_u is the corbel's shear strength; $\delta_0 = 2V_u/K_{c0}$ is the deformation at shear strength; K_{c0} is the corbel's initial stiffness.

The idealized hysteretic model can be fully defined if only shear strength, V_u, and initial stiffness, K_{c0}, are known. A strut-and-tie model also used by [23] is adopted and modified to predict the shear strength, V_u, of deep corbels in the present application. This model leads to Eq. (2) for calculating shear strength. Full details of the strut-and-tie model and how the parameters in Eq. (2) are evaluated are referred to [24].

$$V_u = \sigma_d B l \, \cos\theta \tag{2}$$

where σ_d is the softened compressive strength of concrete; B is the corbel's width; l and θ are the depth and inclination angle of concrete strut, respectively.

For initial stiffness, $K_{c0} = 0.1E_cB$ gives a practically good estimate for the deep corbels in the present tests, where E_c is the elastic modulus of concrete and B is the width of corbel. It was an empirical estimate based on the averaged secant stiffness of the four specimens at 40% ultimate shear strength. With V_u and K_{c0}, the ultimate deformation, δ_0, can be obtained. Fig. 6(b) compares the force–deformation relationships of the four corbels in the test, which are normalized by their respective calculated V_u and δ_0, with idealized skeleton curve. The ratios of test versus calculated shear strengths are between 1.0 and 1.2 for the four specimens.

2.2. Post-tensioned bolts in concrete

The gusset plates on the four specimens were monotonically pulled out by a self-balanced loading system as shown in Fig. 7.
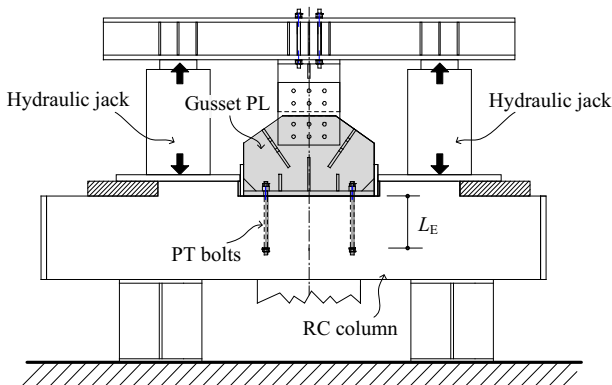
Fig. 7. Loading setup of the tension test on embedded bolts.

Each gusset plate was anchored by four un-bonded bolts that were embedded in the underneath RC column-beam joint and were post-tensioned. The four specimens for the tension tests are referred to as T1–T4. φ16 anchor bolts and SNR490B steel (325 MPa nominal yield strength) were embedded in Specimens T1–T3, while φ13 high-strength bolts (1080 MPa nominal yield strength) were embedded in Specimen T4. The four bolts in the same specimen were post-tensioned to the same tensile force. The total post-tensioning force for each specimen is given in Table 2, along with the embedment length, L_E, of the bolts and the radius of the anchor plate, r (see Fig. 9(a)). For the high-strength bolts in T4, square anchor plates were used instead of circular plates as in the other specimens. For simplicity, an area-equivalent radius, $r = 2b/\sqrt{\pi}$, is used, where $b = 50$ mm is the side length of the square anchor plate.

Specifically designed miniature load cells were mounted between the base plate and the nut for each bolt to monitor the axial force in the bolt, T_b. The total force, T, acting on the gusset plate was obtained from the two hydraulic jacks on both sides. Three LVDTs were used for each specimen to monitor the relative vertical displacement between the base plate and the RC column. The tensile force–displacement relationships and $T - T_b$ relationships are depicted in Fig. 8. Specimens T1–T3 behaved similarly, as expected, while Specimen T4 exhibited higher initial stiffness and sustained greater force at significant stiffness degradation because of its higher post-tensioning force.

The observed behavior of the post-tensioned bolts in concrete can be represented by a simple physical model, as shown in Fig. 9(a), in which an assumingly rigid base plate is compressed by a post-tensioned bolt against the concrete surface. In this model, the anchoring system can be regarded as a combination of two independent springs, that is, a bolt and a concrete spring of stiffness K_b and K_c, respectively. Assuming the concrete remains elastic and the bolt is elastic-perfectly plastic, the force–displacement relationship when the base plate is pulled away from the concrete can be idealized by a trilinear skeleton curve as shown in Fig. 9(b). A detailed derivation of the parameters can be found in Appendix A. It is worth noting that there will be permanent residual deformation once the bolts yield because they cannot be compressed.

Before tensile force is large enough to separate the base plate from the concrete (i.e., zero stress on the interface), the total force, $T = (T_b - T_p)(1 + K_c/K_b)$, where T_b is the bolt force and T_p is the initial post-tensioning force in the bolt. The stiffness ratio, K_c/K_b, can be retrieved by this equation from the test results before separation, which in turn can be used to calibrate the only unknown parameter, θ, in the above model. $\theta = 15°$ gives satisfactory results to match the $T - T_b$ relationship in the tests of all four specimens (Fig. 8(b)). Note that this angle was obtained by fitting the very limited test data without knowing its dependency on the geometrical and material properties of the anchoring system which includes the concrete, the base plate and the bolt. The resultant skeleton curves are superposed on the test results in Fig. 8(a). The higher stiffness of the model, especially after separation, is considered a result of the assumptions that the concrete remains

Table 2
Bolt properties.

	Post-tension (kN)	L_E (mm)	r (mm)
T1	118.6	252	16.0
T2	117.0	252	16.0
T3	121.4	252	16.0
T4	242.0	299	28.2[a]

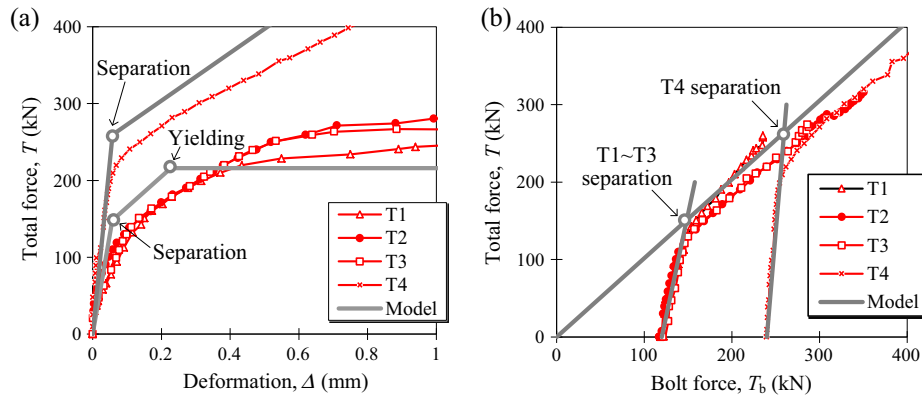[a] Area-equivalent radius of the square anchor plate.

Fig. 8. (a) Bolt force versus total force and (b) deformation versus total force.
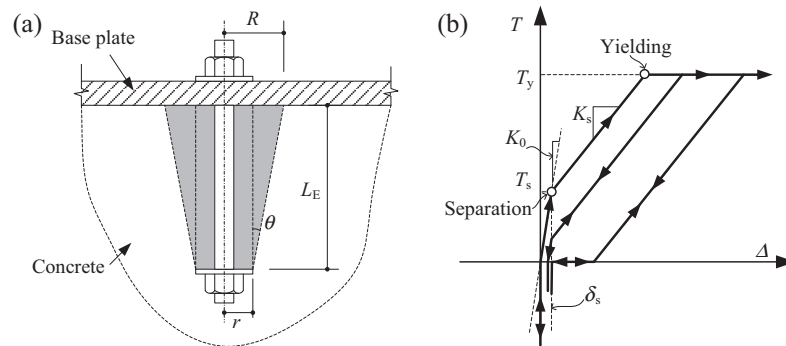

Fig. 9. Models for post-tensioned bolts in concrete: (a) physical model and (b) hysteretic model.

elastic and the gusset plate is rigid. Moreover, the yield strength of the model is lower than those in the tests because the material over-strength is not taken into account.

3. Prototype building and numerical model

A 12-story RC frame with buckling restrained braces in zigzag configuration as shown in Fig. 1 is used as a prototype to investigate the influence of brace connection behavior. The geometrical properties of the building is given in the figure. The middle bay was separated from the rest of the structure and was analyzed in ABAQUS 6.8 [25] as a planar structure. The RC frame was designed for a base shear ratio of 0.3 in compliance with the Japanese seismic provisions for building structures [26,27]. The story weight and cross sectional properties of the RC frame are listed in Table 3. The weight is almost uniformly distributed, and the total weight of the planar frame is 26,509 kN. The axial force at the bottom of the

interior and exterior columns due to gravity is 8380 kN and 5124 kN, approximately 19.3% and 11.8% of their axial strengths, respectively. Beams are modeled by T-section beam elements with top flanges representing the contribution of cast-in-site floor slabs. Rigid zones are adopted for RC beam-column joints. The widths of equivalent beam flanges and the rigid zones are determined in accordance with the AIJ standard for design of concrete structures [28].

Although the beams in the middle span are eliminated to give way to the BRB gusset connections, elastic springs are added in the positions of the removed beams to represent the axial stiffness of the floor slab and any secondary beams out of the analysis plane. The RC beams and columns are modeled by fiber beam elements with user-defined uniaxial hysteresis for concrete and reinforcement fiber [29]. Shear failure of these members is not modeled. BRBs are modeled by truss elements with elastic-perfectly plastic hysteresis, which takes into account the over-strength and increased stiffness of the elastic segments on both ends. In order

Table 3
Story weight and cross sectional properties of the RC columns and beams.

Floor	Story weight	f_c'	Beam section			Column section		
	(kN)	(MPa)	b (mm)	h (mm)	ρ_s (%)[a]	b (mm)	h (mm)	ρ_s (%)[b]
11, 12	2395	30	600	900	0.92	850	850	1.76
9, 10	2086	36	600	900	1.11	900	900	1.89
7, 8	2161	36	600	900	1.11	950	950	2.02
4, 5, 6	2172	42	600	900	1.11	950	950	2.02
1, 2, 3	2237	48	600	1000	1.00	950	950	2.38
Foundation		42	600	2500	LE[c]			

[a] Tensile reinforcement ratio.
[b] Whole section reinforcement ratio.
[c] Foundation beam is assumed linear elastic in the analysis.

not to impose too large an additional axial force on columns, the expected strength (including over-strength) of all the six BRBs is assumed to be identical at 2100 kN. Although more sophisticated BRB strength distributions are possible, they are considered unnecessary for the current case study where the number of BRBs are small. More importantly, identical BRBs would help clarify the sources of loads on gusset connections. For the same reason, the difference in BRB's tensile and compressive strengths is not modeled. A mass proportional damping model is used, and a 2% damping ratio is assigned for the 1st mode e.g., [30].

Three ground motion records as listed in Table 4 were selected for the analysis, where D is the Joyner–Boore distance and T_S is the significant duration. All records were normalized by peak ground velocity (PGV) to PGV = 50 cm/s, which is a well-accepted intensity level in Japan for assessing the seismic performance of tall buildings or buildings equipped with dampers through time history analyses. As can be observed in the response spectra in Fig. 10, the Takatori and JMA Kobe records represent near-fault ground motions with significant medium- or long-period components, while the MYG012-EW record contains significant short-period components.

4. Influence of nonlinearity of BRB connections

Taking advantage of the zigzag configuration that separates shear and tensile resistances, brace connections can be modeled by user-defined dimensionless bi-axial spring elements. The element is simply a combination of two orthogonal uniaxial springs, one for corbels above and below the gusset plate and the other for post-tensioned bolts (Fig. 11). Node 1 of the element belongs to the column-beam rigid joint; Node 2 is shared by the truss elements representing BRBs. The two nodes share the same coordinates. The above-mentioned additional elastic spring element
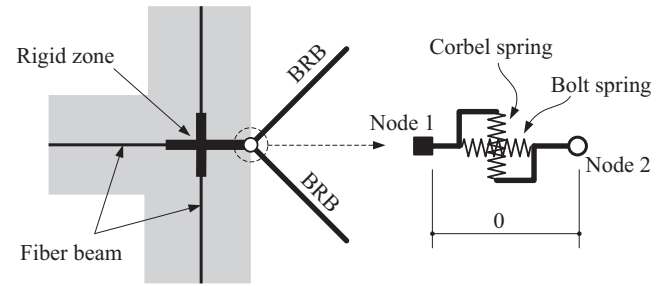
Table 4
Properties of selected ground motions.

ID	Earthquake	M_w	D (km)	T_S (s)
Takatori-NS	Kobe, 1995	6.9	1.46	11.3
JMA Kobe-NS	Kobe, 1995	6.9	0.94	8.4
MYG012-EW	Tohoku, 2011	9.0	168[a]	103.1

[a] Epicenter distance.

Fig. 10. Velocity spectra of selected ground motion records.

Fig. 11. User-defined bi-axial spring element for proposed BRB connection.

representing the axial stiffness of the slab and secondary beams is connected to Node 1 so that it has no contribution to either the strength or stiffness of the brace connection. The hysteretic models of the two springs are already described in Figs. 6 (a) and 9(b).

The upper-bound horizontal force that can develop in bolt connections is the sum of the horizontal components of BRBs' strength, which is approximately 3187 kN for the prototype building. Although the connection is supposed to sustain only marginal tensile force, this upper-bound force is taken as a conservative estimate of the strength demand for post-tensioned bolts. Either of the following two design objectives can be adopted in proportioning the bolts and determining the post-tensioning force: (1) no separation is allowed or (2) no yielding is allowed at the strength demand. 8 ϕ26 high-strength steel bolts, each of which is allowed to be post-tensioned to 457 kN, are selected to satisfy the first objective. According to the equations in Appendix A, a post-tensioning force of 367 kN for each bolt gives an overall separation force exactly the same as the upper-bound strength demand. For the second objective, 8 ϕ23 high-strength steel rods, each post-tensioned to 93 kN, would be sufficient. The first design of the bolts is referred to as 'standard bolts' or 'ST' and the second as 'looser bolts' or 'LS', hereinafter.

The shear demand for concrete corbels is limited by the sum of the vertical components of BRBs' strength. Corbel brittle failure should be avoided to ensure BRB's energy dissipation. Based on the above-mentioned strut-and-tie model, a concrete corbel of 200 mm by 850 mm by 850 mm in dimensions and 30 MPa in concrete compressive strength, reinforced by ϕ19 stirrups at 100 mm interval, may provide shear strength of 3378 kN, approximately 1.2 times the shear demand. The initial stiffness of such a corbel is about 2167 kN/mm (i.e., $0.1E_cB$ according to the tests). It is referred to as 'standard corbel', hereinafter. Another two artificial corbel cases are conceived for comparison purposes. In the 'stiffer corbel' case, the initial stiffness of the corbel is assumed to be twice that of the standard corbel while all other properties remain the same. In the 'elastic corbel' case, the hysteresis of the corbel is assumed to be nonlinear elastic instead of inelastic as in Fig. 6(a), and the skeleton curve remains the same. In other words, the corbel may unload exactly along the skeleton curve and there is no residual deformation.

Five different sets of connection properties combining different corbel and bolt cases are listed in Table 5. Correspondingly, nonlin-
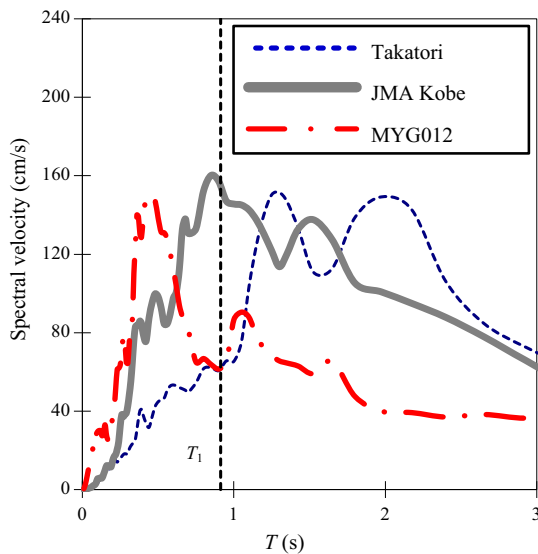
Table 5
Analysis cases.

ID	Corbels	Bolts	R_s
B-ST	Rigid	Standard	169.8
B-LS	Rigid	Looser	9.6
C-ST	Standard	Standard	13.2
C-RG	Stiffer	Standard	24.5
C-EL	Elastic	Standard	13.2

ear time-history analyses were conducted on five prototype buildings, each with a different set of connection properties. The stiffness of the post-tensioned bolts and corbels can be projected to the axial direction of BRBs so that an equivalent brace stiffness can be evaluated. A connection stiffness ratio, R_s, which is the ratio of the bolt-and-corbel connection's projected stiffness to the BRB's axial stiffness, is used to compare the connection stiffness in the different analysis cases. The ratios are calculated by Eq. (3). Their values in the five analysis cases are listed in Table 5. The analysis cases adopted herein cover a wide range of R_s from more than 100 in the B-ST case to less than 10 in the B-LS case.

$$R_s = \frac{1}{\left(\frac{\sin^2 \alpha}{K_{ct}} + \frac{\cos^2 \alpha}{K_{bt}}\right) \cdot K_{BRB}} \tag{3}$$

where K_{BRB} and α is the axial stiffness and inclination angle of BRB, respectively; K_{ct} is the tangent stiffness of concrete corbels at the shear demand; K_{bt} is the tangent stiffness of post-tensioned bolts at the upper-bound tensile demand, that is, K_0 for B-ST case (no separation) and K_s for B-LS case (separated but no yielding).

The maximum deformation in bolts and that in corbels are illustrated in Fig. 12. The separation of post-tensioned bolts substantially increases the maximum deformation in the bolts (B-ST versus B-LS), and the deformation distribution varies from record to record. The distribution indicates the dynamic nature of the horizontal force in the bolt connections and that the horizontal components of the neighboring BRBs do not cancel each other out; significant tensile force can develop in the bolt connection. This will be discussed later. For concrete corbels, the maximum deformation is proportional to the stiffness, and its distribution is practically independent of the ground motion records. A bold gray curve is superimposed in Fig. 12(b) to show the estimated static corbel deformation at the shear demand for the C-ST case. It matches well with the dynamic analysis results in the medium- and lower-stories where the BRBs are well yielded.

Fig. 13(a) compares the maximum inter-story drift ratios (IDR) of the counterpart moment-resisting frame (MRF) and the zigzag BRBFs with various brace connection properties. Although the connection flexibility somewhat increases the maximum IDR, the increase is generally insignificant compared to the reduction of the maximum IDR by implementing the bracing system. Fig. 13(b) compares the absolute difference between the
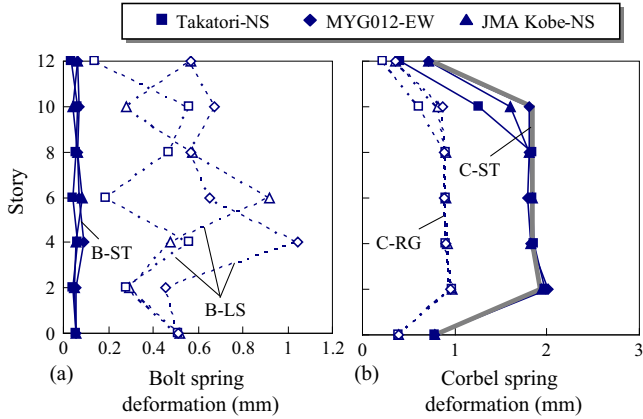

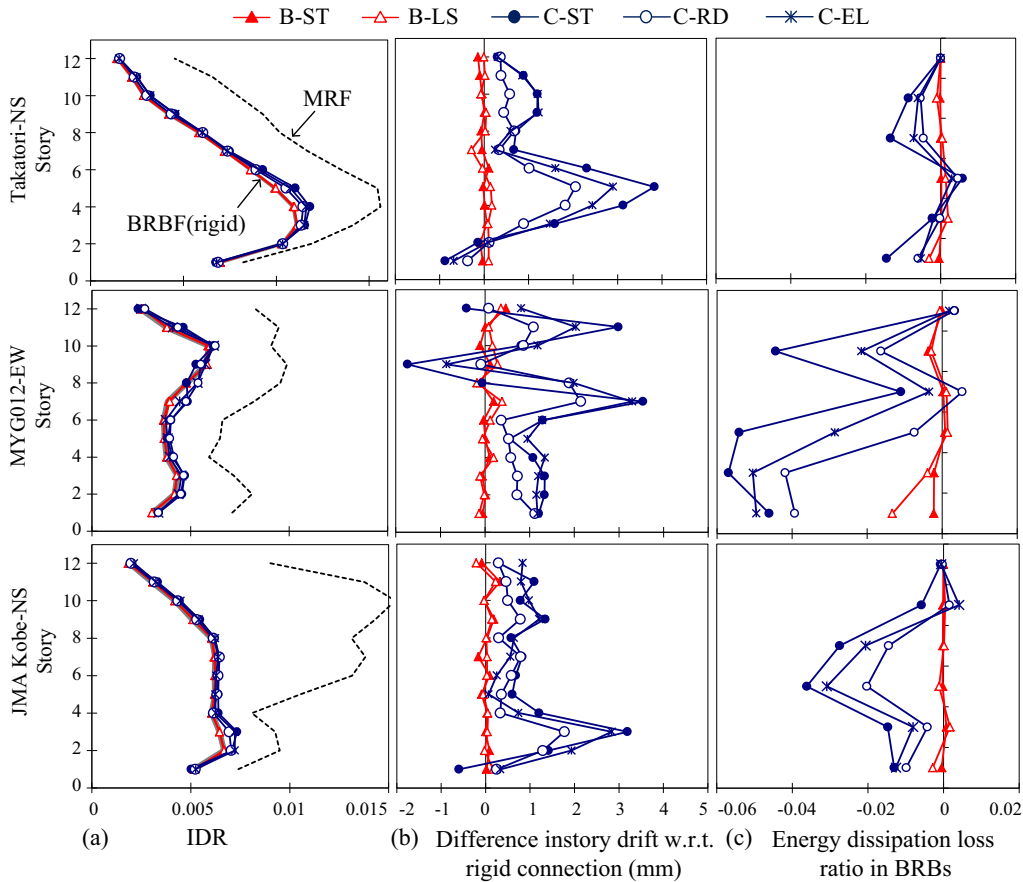**Fig. 12.** Maximum deformations of the connection.

Fig. 13. Deformation and energy dissipation results.

maximum IDR with nonlinear BRB connections and that with rigid connections. The influence of post-tensioned bolts seems negligible even if gusset plates separate with concrete members (e.g., the B-LS case). The increase in IDR can be attributed to the deformation of concrete corbels. The difference in IDRs is practically proportional to the corbel stiffness. Residual deformation also has an effect but not as significant as that of initial stiffness. Similar observations can be made upon the energy dissipation loss ratio in BRBs (Fig. 13(c)). It is defined as the ratio of the reduction in BRB hysteretic energy dissipation because of connection nonlinearity to the total hysteretic energy dissipation of BRBs with rigid connections.

5. Influence of higher mode vibration

While displacements are not likely to be influenced significantly by higher modes, higher modes may significantly influence internal forces. As is shown in Fig. 13(a), the difference in both inter-story drift and energy dissipation between B-ST and B-LS cases is negligible, in spite of the fact that the bolt connections in B-LS case sustain much larger deformation than that in B-ST case. This suggests that the horizontal force developed in bolt connections may be a result of higher mode vibrations un-synchronized with building's the peak inter-story drift. This is evident in Fig. 14, which compares the time history during 2–5 s of the inter-story drift at the 6th floor and that of the forces in the BRB connection at the same floor. The peak story drifts, as indicated by hollow circles in the figure, take place when the vertical force is at its maximum and the horizontal force is very small. In other words, there is a phase difference between the peak story drift and peak horizontal force.

Fig. 14 also shows that the maximum horizontal force imposed on the bolt connection can become as large as the strength of a single BRB. Such significant horizontal force should not occur if

the structure vibrates in only its first mode. To validate the possible influence of higher mode vibration, the axial forces of BRBs, $\mathbf{f}(t)$, are expanded as the summation of its modal forces, $\mathbf{f}_i(t)$, as in Eq. (4).

$$\mathbf{f}(t) = \sum_{i=1}^{n} \mathbf{f}_i(t) = \sum_{i=1}^{n} F_i(t) \boldsymbol{\varphi}_{\mathrm{fi}} \tag{4}$$

where $\boldsymbol{\varphi}_{\mathrm{fi}}$ is the BRB modal force shape vector corresponding to the ith mode; $F_i(t)$ is the time variance of the ith modal force, $\mathbf{f}_i(t)$.

By assuming a diagonal mass matrix, $\mathbf{M}$, with identical diagonal elements, the shape vectors, $\boldsymbol{\varphi}_{\mathrm{fi}}$, are approximately orthogonal to each other, that is, $\boldsymbol{\varphi}_{\mathrm{fi}}^T \mathbf{M} \boldsymbol{\varphi}_{\mathrm{fj}} = 0$ $(i \neq j)$. By multiplying Eq. (4) by $\boldsymbol{\varphi}_{\mathrm{fi}}^T \mathbf{M}$, it gives Eq. (5) to calculate the ith modal force of a BRB.

$$\mathbf{f}_i(t) = F_i(t) \boldsymbol{\varphi}_{\mathrm{fi}} = \frac{\boldsymbol{\varphi}_{\mathrm{fi}}^T \mathbf{M} \mathbf{f}(t)}{\boldsymbol{\varphi}_{\mathrm{fi}}^T M \boldsymbol{\varphi}_{\mathrm{fi}}} \boldsymbol{\varphi}_{\mathrm{fi}} \tag{5}$$

Fig. 15 depicts the 1st and 2nd modal forces obtained by Eq. (5) of the upper BRB connecting to the 6th floor. The modal forces obtained by the nonlinear (NL) dynamic analysis are compared with those obtained by the linear elastic (LE) analysis. The 1st mode BRB force is suppressed by yielding while the 2nd mode force in nonlinear analysis remains comparable to that in linear elastic analysis. The maximum force of the 2nd mode is only 16% of that of the 1st mode in the linear elastic analysis, while this ratio grows up to 87% in nonlinear analysis. In the 2nd mode, neighboring BRBs in some stories may deform in the same direction, i.e., both in tension or in compression. This may lead to significant horizontal force demand for the bolt connection, as observed in Fig. 14. Such effects of higher modes on both the magnitudes and distribution of internal forces have been observed and reported in previous research for either slender shear walls [31,32] or moment resisting frames even if the first mode dominates the vibration [33].
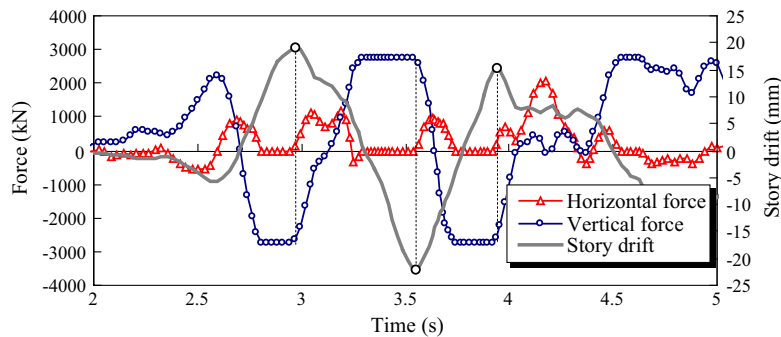

Fig. 14. Time history of horizontal and vertical forces in BRB connection at the 6th floor of zigzag BRBF with rigid BRB connections under JMA Kobe-NS record.
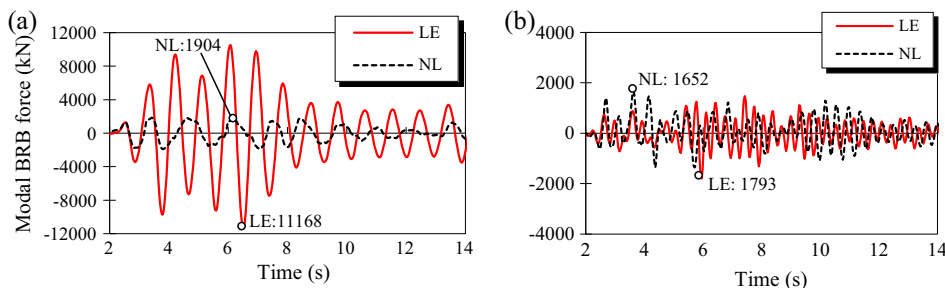

Fig. 15. Modal decomposition of the axial force of the upper BRB connecting to the 6th floor under the JMA Kobe-NS: (a) 1st mode and (b) 2nd mode.
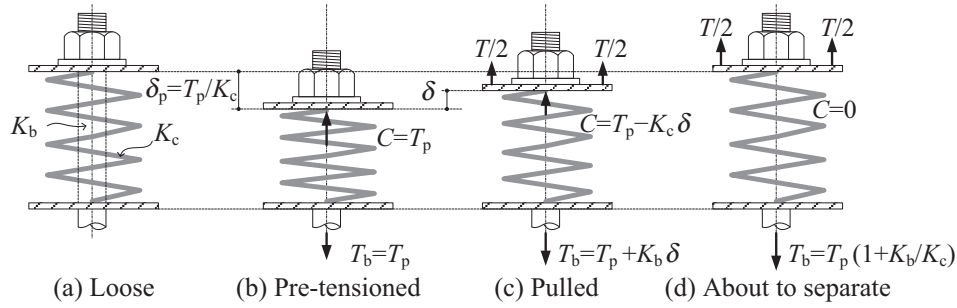
Fig. A.1. Tensile behavior of post-tensioned bolt embedded in concrete before separation.

6. Conclusions

Using a zigzag buckling restrained braced frame provides a system-level solution for implementing BRBs in RC structures, featuring more reliable and easy-to-design gusset connections. The proposed connection consists of a pair of concrete corbels for shear resistance and a group of post-tensioned bolts for tensile resistance. Experimental tests were conducted on concrete corbels and post-tensioned bolts with the purpose of establishing a practical and realistic numerical model for the proposed connection. For concrete corbels, a strut-and-tie model is used to estimate its shear strength, while approximate estimates are made for its stiffness with the assistance of the test results. For post-tensioned bolts, a trilinear skeleton model is calibrated to describe the separation of the compressed interface and the bolt yielding.

The influences of nonlinearity of BRB connections on the seismic responses of the proposed system are assessed through nonlinear time-history analysis. The bolt-and-corbel connections for BRBs in the prototype building are proportioned according to the models derived from the test results to make sure that the selected properties are reasonable and practical.

Five analysis cases with different sets of connection properties are studied to show that the flexibility of concrete corbels may lead to an increase in the inter-story drift of the entire building. The elastic deformation of post-tensioned bolts has little effect on the global responses, because the fact that the local tensile force in bolts arises from higher mode vibrations and does not coincide with peak inter-story drifts of the building. Higher mode effects are also responsible for the significant tensile force demand on the bolt connection, which may be overlooked from a static point of view and may lead to unsafe bolt design.

Acknowledgements

Appendix A

The parameters necessary for the trilinear skeleton curve (Fig. 9 (b)) for post-tensioned bolts embedded in concrete are defined herein. As mentioned above, the anchoring system is regarded as a combination of a bolt spring of axial stiffness, K_b, and a concrete spring of axial stiffness, K_c (Fig. A.1(a)) Upon post-tensioning, an initial tensile force, T_p, is imposed in the bolt and at the same time

the concrete spring is compressed by a deformation, $\delta_p = T_p/K_c$, assuming the concrete spring is elastic (Fig. A.1(b)). When the system is pulled by a tensile force, T, to have a deformation of δ, the bolt tension, T_b, increases and the concrete compression, C, decreases (Fig. A.1(c)). Force equilibrium gives $T = T_b - C = (K_b + K_c) \delta$. In other words, the initial stiffness of a post-tensioned bolt, K_0, is the sum of bolt and concrete stiffness (Eq. (A.1)). When the tensile force, T, increases to impose a deformation, $\delta = \delta_p$, the concrete compression, C, becomes zero and the compressed interface is about to separate. At this instant, the bolt force, T_b, equals the external force T, which is also referred to as the separation force, T_s (Eq. (A.3)). The corresponding deformation at separation is $\delta_s = T_s/K_0$.

$$K_0 = K_b + K_c \tag{A.1}$$

where $K_b = A_b E_s/L_E$ is the bolt axial stiffness, A_b is the bolt cross section area, E_s is the steel elastic modulus, L_E is the bolt embedment length (see Fig. 9(a)); K_c is the effective stiffness of the underneath concrete, which is taken as the axial stiffness of a hollow cone frustum (see Fig. 9(a)). Eq. (A.2) gives a practically good estimate of this stiffness.

$$K_c = (\pi r R - A_b) E_c / L_E \tag{A.2}$$

where r is the radius of the base anchor plate; $R = r + L_E \tan\theta$ is the top radius of the frustum, E_c is the concrete elastic modulus.

$$T_s = T_p \left(1 + \frac{K_b}{K_c}\right) \tag{A.3}$$

After separation, the embedded bolt in tension becomes a system of the bolt and concrete springs in series, whose stiffness is given in Eq. (A.4). The bolt yield force can be conservatively taken as $T_y = A_b f_y$, in which f_y is the nominal yield strength of the bolt steel.

$$K_s = \frac{K_b K_c}{K_b + K_c} \tag{A.4}$$

References

[1] AISC. Specification for structural steel buildings. ANSI/AISC 360-05. American Institute of Steel Construction. Chicago, IL; 2002.
[2] Kishiki S, Yamada S, Wada A. Experimental evaluation of structural behavior of gusset plate connection in BRB frame system. In: Proc 14th world conference on earthquake engineering, Beijing; 2008 [in CD-ROM].
[3] Chou CC, Liu JH, Pham DH. Steel buckling-restrained braced frames with single and dual corner gusset connections: seismic tests and analyses. Earthquake Eng Struct Dynam 2012;41(7):1137–56.
[4] Tsai KC, Hsiao PC, Wang KJ, Weng TT, Lin ML, Lin KC, et al. Pseudo-dynamic tests of a full-scale CFT/BRB frame – part I: specimen design, experiment and analysis. Earthquake Eng Struct Dynam 2008;37(7):1081–98.
[5] Sabelli R, Mahin S, Chang C. Seismic demands on steel braced frame buildings with buckling-restrained braces. Eng Struct 2003;25(5):655–66.
[6] Ariyaratana C, Fahnestock LA. Evaluation of buckling-restrained braced frame seismic performance considering reserve strength. Eng Struct 2011;33 (1):77–89.

[7] Maheri MR, Ghaffarzadeh H. Connection overstrength in steel-braced RC frames. Eng Struct 2008;30(7):1938–48.

[8] Gu LZ, Gao XY, Xu JW, et al. Research on seismic performance of BRB concrete frames. J Build Struct 2011;32(7):101–11 [in Chinese].

[9] Maheri MR, Hadjipour A. Experimental investigation and design of steel brace connection to RC frame. Eng Struct 2003;25(13):1707–14.

[10] Li GQ, Guo XK, Sun FF, Chen C. Study of the anchorage connections for buckling restrained braces. Part 1: experimental investigation. Adv Struct Eng 2013;16 (4):759–72.

[11] Ishii T, Mukai T, Kitamura H, et al. Seismic retrofit for existing R/C building using energy dissipative braces. In: Proc 13th world conference on earthquake engineering; 2004 [in CD-ROM, paper No. 1209].

[12] Yokouchi H, Kitajima K, Ageta H, Chikui H, Nakanishi M, Adachi H. Pseudo-dynamic test on an existing R/C school building retrofitted with friction dampers. In: Proc 13th world conference on earthquake engineering; 2004 [in CD-ROM, paper No. 2111].

[13] Di Sarno L, Manfredi G. Seismic retrofitting with buckling restrained braces: application to an existing non-ductile RC framed building. Soil Dynam Earthquake Eng 2010;30(11):1279–97.

[14] Di Sarno L, Manfredi G. Experimental tests on full-scale RC unretrofitted frame and retrofitted with buckling restrained braces. Earthquake Eng Struct Dynam 2012;41(2):315–33.

[15] Ichikawa Y, Okayasu T, Nakamura H, Yamada S, Wada A. Experimental study on joint of seismic retrofitting brace for steel structure using shear-key plate adhered to concrete slab. J Struct Constr Eng, Trans AIJ 2005;596:133–40 [in Japanese].

[16] Benavent-Climent A, Oliver-Saiz E, Donaire-Avila J. New connection between reinforced concrete building frames and concentric braces: shaking table tests. Eng Struct 2015;96:7–21.

[17] Maegawa T, Qu Z, Kishiki S, Maida Y, Hamada M, Sakata H. Local damage control of unconstrained gusset connection for buckling restrained braces in RC frames. In: Proc IABSE conference, Nara; 2015.

[18] Berman JW, Bruneau M. Cyclic testing of a buckling restrained braced frame with unconstrained gusset connections. J Struct Eng, ASCE 2009;135 (12):1499–510.

[19] Khampanit A, Leelataviwat S, Kochanin J, Warnitchai P. Energy-based seismic strengthening design of non-ductile reinforced concrete frames using buckling-restrained braces. Eng Struct 2014;81:110122.

[20] Wada A, Nakashima M. From infancy to maturity of buckling restrained braces research. In: Proc 13th world conference on earthquake engineering; 2004 [in CD-ROM, paper No. 1732].

[21] Maida Y, Kishiki S, Nonoyama M, Qu Z, Maegawa T, Hamada M, Sakata H, Wada A. Experimental evaluation of structural behavior of RC frame subassemblies with BRB connections. J Struct Constr Eng, Trans AIJ 2012;77(681):1737–46 [in Japanese].

[22] Qu Z, Kishiki S, Sakata H, Wada A, Maida Y. Sub assemblage cyclic loading test of RC frame with buckling restrained braces in zigzag configuration. Earthquake Eng Struct Dynam 2013;42(7):1087–102.

[23] Russo G, Venir R, Pauletta M, Somma G. Reinforced concrete corbels – shear strength model and design formula. ACI Struct J 2006;103(1):3–10.

[24] Qu Z, Maida Y, Kishiki S, Sakata H. Shear resistance of a type of reinforced concrete corbels for shear keys. In: Proc 9th Intl Conf Urban Earthquake Eng (9CUEE) & 4th Asia Conf Earthquake Eng (4ACEE), Tokyo, Japan; 2012 [paper No. 04-231].

[25] Dassault Systèmes Simulia Corp., Providence, RI, USA.

[26] BCJ. The building standard law of Japan. The Building Center of Japan; 2004 [in Japanese].

[27] AIJ. Design guidelines for earthquake resistant reinforced concrete buildings based on inelastic displacement concept. Architectural Institute of Japan; 1999 [in Japanese].

[28] AIJ. Standard for structural calculation of reinforced concrete structures. Architectural Institute of Japan; 2010. p. 63–70, 87–89 [in Japanese].

[29] Qu Z, Ye LP. Strength deterioration model based on effective hysteretic energy dissipation for RC members under cyclic loading. In: Proc 7th Int Conf Urban Earthquake Eng (7CUEE), Tokyo, Japan; 2010. p. 851–6.

[30] Elnashai AS, Di Sarno L. Fundamentals of earthquake engineering. UK: Wiley and Sons; 2008.

[31] Eibl J, Keintzel E. Seismic shear forces in RC cantilever shear walls. In: Proc 9th World conference on earthquake engineering; 1988, vol. VI, p. 5–10.

[32] Panagiotou M, Restrepo JI. Dual-plastic hinge design concept for reducing higher-mode effects on high-rise cantilever wall buildings. Earthquake Eng Struct Dynam 2009;38(12):1359–80.

[33] Maniatakis C, Psycharis IN, Spyrakos CC. Effect of higher modes on the seismic response and design of moment-resisting RC frame structures. Eng Struct 2013;56:417–30.